https://doi.org/10.5194/gmd-2020-113
Preprint. Discussion started: 24 June 2020
© Author(s) 2020. CC BY 4.0 License.

Geoscientific Model Development Discussions

Potential yield simulated by Global Gridded Crop Models: a process-based emulator to explain their differences

Bruno Ringeval[1]*, Christoph Müller[2], Thomas A.M. Pugh[3], Nathaniel D. Mueller[4], Philippe Ciais[5], Christian Folberth[6], Wenfeng Liu[5], Philippe Debaeke[7], Sylvain Pellerin[1]

[1] ISPA, Bordeaux Sciences Agro, INRAE, 33140, Villenave d'Ornon, France

[2] Potsdam Institute for Climate Impact Research, Member of the Leibniz Association, Potsdam, Germany

[3] School of Geography, Earth & Environmental Science and Birmingham Institute of Forest Research, University of Birmingham, Birmingham, United Kingdom

[4] Department of Earth System Science, University of California, Irvine, CA, USA

[5] Laboratoire de Sciences du Climat et de l'Environnement, LSCE/IPSL, CEA-CNRS-UVSQ, Université Paris-Saclay, Gif-sur-Yvette, France

[6] Ecosystem Services and Management Program, International Institute for Applied Systems Analysis, 2361 Laxenburg, Austria

[7] AGIR, University of Toulouse, INRAE, 31326, Castanet-Tolosan, France

* corresponding author: Bruno Ringeval, bruno.ringeval@inrae.fr

https://doi.org/10.5194/gmd-2020-113
Preprint. Discussion started: 24 June 2020
© Author(s) 2020. CC BY 4.0 License.

Geoscientific Model Development Discussions

20 **Abstract**

How Global Gridded Crop Models (GGCMs) differ in their simulation of potential yield and reasons for those differences have never been assessed. The GGCM Inter-comparison (GGCMI) offers a good framework for this assessment. Here, we built an emulator (called SMM for Simple 25 Mechanistic Model) of GGCMs based on generic and simplified formalism. The SMM equations describe crop phenology by a sum of growing degree days, canopy radiation absorption by the Beer-Lambert law, and its conversion into aboveground biomass by a radiation use efficiency (*RUE*). We fitted the parameters of this emulator against gridded aboveground maize biomass at the end of the growing season simulated by eight different GGCMs in a given year (2000). Our 30 assumption is that the simple set of equations of SMM, after calibration, could reproduce the response of most GGCMs, so that differences between GGCMs can be attributed to the parameters related to processes captured by the emulator. Despite huge differences between GGCMs, we show that if we fit both a parameter describing the thermal requirement for leaf emergence by adjusting its value to each grid-point in space, as done by GGCM modellers following the GGCMI protocol, 35 and a GGCM-dependent globally uniform *RUE*, then the simple set of equations of the SMM emulator is sufficient to reproduce the spatial distribution of the original aboveground biomass simulated by most GGCMs. The grain filling is simulated in SMM by considering a fixed in time fraction of net primary productivity allocated to the grain (*frac*) once a threshold in leaves number (n_{thresh}) is reached. Once calibrated, these two parameters allow to capture the relationship between 40 potential yield and final aboveground biomass of each GGCM. It is particularly important as the divergence among GGCMs is larger for yield than for aboveground biomass. Thus, we showed that the divergence between GGCMs can be summarized by the differences in few parameters. Our simple but mechanistic model could also be an interesting tool to test new developments in order to improve the simulation of potential yield at the global scale.

https://doi.org/10.5194/gmd-2020-113
Preprint. Discussion started: 24 June 2020
© Author(s) 2020. CC BY 4.0 License.

Geoscientific Model Development Discussions

1. Introduction

Potential yield corresponds to the yield achieved when an adapted crop cultivar grows in non-limiting environmental conditions (i.e. without water and nutrient stresses and in the absence of damages from weeds, pests and diseases) under a given crop management (e.g. plant density). Fundamentally, it is determined by a reduced number of environmental variables: prevailing radiation, temperature and atmospheric CO_2 concentration. Biotic variables such as cultivar characteristics (e.g. maturity group, leaf area index, root depth, harvest index), plant density and sowing date modulate how the environmental conditions are converted into yield. At local scale (field, farm or small region), potential yields can be estimated from field experiments, yield census, or by crop growth models (Lobell et al., 2009). Crop simulation models provide a robust approach because they account for the interactive effects of genotype, weather, and management (van Ittersum et al., 2013). These models are mathematical representations of our current understanding of biophysical crop processes (phenology, carbon assimilation, assimilate allocation) and of crop responses to environmental factors. Such models have been designed to separate genotype * environment * management interactions, for example by factorial simulations where one driver is varied at a time. Models require site-specific inputs, such as daily weather data, crop management practices (sowing date, cultivar maturity group, plant density, fertilization and irrigation amounts and dates), and soil characteristics; with some of them being not useful in the purpose to simulate potential yield. At local scale, crop models can be calibrated to account for local specificities, in particular for specificities related to the cultivar used at these sites (Grassini et al., 2011)

Potential yield is also a variable of interest at large (country, global) spatial scales, in particular as it is required for yield gap analyses (van Ittersum et al., 2013; Lobell et al., 2009). Such analyses are necessary to get a large-scale picture of yield limitations and to investigate questions related to production improvement strategies, food security and management of resources with a global perspective. However, while crop models used at local scale can be calibrated to account for local specificities, it is much more complicated to model the spatial variations of yields at the global scale. Local crop models have been applied at the global scale either directly or through the implementation of some of their equations into global vegetation models (Elliott et al., 2015). Global Gridded Crop Models (GGCMs in the following) provide spatially explicit outputs, typically at half degree resolution in latitude and longitude. Their simulations are prone to uncertainty. In particular, it is quite difficult to get reliable information about the diversity of cultivars (Folberth et al., 2019) or crop management at the global scale with large effects on the crop behavior (Drewniak

https://doi.org/10.5194/gmd-2020-113
Preprint. Discussion started: 24 June 2020
© Author(s) 2020. CC BY 4.0 License.

Geoscientific Model Development Discussions

et al., 2013).

Increasing our confidence in potential yield simulated by GGCMs is required to improve our ability in replying to societal questions mentioned above. To do so, we need first to understand how and why GGCMs potentially diverge in potential yield simulation. The GGCM Inter-comparison (GGCMI phase I) provides a framework relevant to investigate the differences between GGCMs, as all GGCM modellers followed the same protocol (Elliott et al., 2015). Model outputs are available on the GGCMI data archive (Müller et al., 2019a). In the GGCMI framework, a simulation performed with harmonized growing period, absence of nutrient stress and irrigated conditions (see below) is particularly adapted to simulate potential yield. Figure 1 displays, for maize, the average and coefficient of variation (CV) of such simulated aboveground biomass (*biom*) and yield (*grain*) among 8 GGCMs participating to GGCMI that have been used in our following analysis. While the GGCM divergence under potential conditions is lower than the GGCM divergence when limiting factors are represented (Fig.S2), it remains relatively high. Figure 1 shows that the CV in potential conditions is higher for *grain* than for *biom* and the CV for *grain* can reach locally more than 50%. To understand what could explain these differences, we built a mechanistic emulator of GGCMs based on generic processes controlling the accumulation of biomass (phenology from the sum of growing degree days, light absorption, radiation use efficiency) and the transformation of biomass into grain yield (trigger of yield formation, allocation of net primary production (NPP) to yield). We then calibrated the parameters of the emulator independently for each GGCM against GGCM simulated *biom* and GGCM simulated relationship between *biom* and *grain*. Our assumption is that a simple set of equations, with calibrated parameters, can reproduce the outputs of most GGCMs and could be used to explore the sources of differences between them. We choose to use a process-based (even if very simple) model as we expect that this model could propose interesting perspectives as explained in the Discussion. In particular, if able to reproduce the results of an ensemble of GGCMs, it could be an alternative to the model ensemble mean or median usually used in inter-comparison exercises (Martre et al., 2015). Running much faster than GGCMs, it would also be an interesting tool to test new developments, such as the implementation of cultivar diversity, to improve the simulation of potential yield at the global scale.

https://doi.org/10.5194/gmd-2020-113
Preprint. Discussion started: 24 June 2020
© Author(s) 2020. CC BY 4.0 License.

Geoscientific Model Development Discussions

2. Methods

2.1. GGCM emulator

For any given day *d* of the growing season (defined here as the period between the planting day, t_p, and the crop maturity, t_m), we used the equations 1-7 which rely on concepts commonly used in modelling of ecosystem productivity to compute the potential aboveground biomass (*biom*, in t DM ha^{-1}). Variables and parameters are summarized in Table 1 and a simplified flow chart is given in Fig.S3.

For any *d* in [t_p, t_m], the thermal time (*TT*) is computed from the daily mean temperature (*tas*, in °C) by using a reference temperature (T_0):

$$TT(d) = tas(d) - T_0 \qquad \text{(Eq.1)}$$

GDD is the sum of growing degree days, defined as follows:

$$GDD(d) = \sum_{i \le d} max(0,\ TT(i)) \qquad \text{(Eq.2)}$$

The number of leaves per plant (n_{leaf}) is computed from *GDD* and one parameter representing the thermal requirement for the emergence of any leaf (GDD_{1leaf}):

$$n_{leaf}(d) = min(max_{nleaf},\ GDD(d)/GDD_{1\,leaf}) \qquad \text{(Eq.3)}$$

where max_{nleaf} is the maximum number of leaves. In our model, as soon as one leaf emerges, we assumed that it reaches its fully expanded leaf area, which is the same for all leaves (individual leaf area, called S_{leaf} hereafter). The incoming photosynthetic active radiation (PAR_{inc}) is derived from the short-wave downwelling radiation (*rsds* in MJ m^{-2} day^{-1}) and its active fraction, *f*:

$$PAR_{inc}(d) = f * rsds(d) \qquad \text{(Eq.4)}$$

The absorbed *PAR* by the canopy (*APAR*) is determined by assuming an exponential function according to the Beer-Lambert law:

$$APAR(d) = PAR_{inc}(d) * (1 - \exp(-C * n_{leaf}(d))) \qquad \text{(Eq.5)}$$

where *C* is a constant (see below). The Net Primary Productivity dedicated to the aboveground biomass (NPP_{biom}) is computed from *APAR* with a constant Radiation Use Efficiency (*RUE* in g DM MJ^{-1}):

$$NPP_{biom}(d) = RUE * APAR(d) \qquad \text{(Eq.6)}$$

The aboveground biomass corresponds to the sum over time of NPP_{biom}:

$$biom(d) = \sum_{i \le d} (NPP_{biom}(i)) \qquad \text{(Eq.7)}$$

https://doi.org/10.5194/gmd-2020-113
Preprint. Discussion started: 24 June 2020
© Author(s) 2020. CC BY 4.0 License.

Geoscientific Model Development Discussions

The parameter C of Eq.5 can be decomposed in different parameters:

$$C = k * S_{leaf} * d_{plant} \quad \text{(Eq.8)}$$

with k is the light extinction coefficient, S_{leaf} is the individual leaf area and d_{plant} is the plant density. The product of S_{leaf}, d_{plant} and the number of leaves of a given day d (i.e. $n_{leaf}(d)$), corresponds to the Leaf Area Index (LAI) of the same day, i.e.:

$$LAI(d) = S_{leaf} * d_{plant} * n_{leaf}(d) \quad \text{(Eq.9)}$$

in such a way that Eq.5 can be re-written as:

$$APAR(d) = PAR_{inc}(d) * (1 - \exp(-k * LAI(d))) \quad \text{(Eq.5bis)}$$

We preferred Eq.5 instead of Eq.5bis as we cannot calibrate separately the different parameters composing C and because we do not have any information about the LAI from GGCMs (see discussion).

To compute the grain biomass at maturity, we first define the day k such as :

$$n_{leaf}(k) \geq n_{thresh} \quad \text{(Eq.10)}$$

From day k, a fixed fraction ($frac$) of NPP_{biom} constitutes the Net Primary Productivity dedicated to the variable *grain* (called NPP_{grain}):

$$\begin{cases} \text{If } d \geq k, & NPP_{grain}(d) = frac * NPP_{biom}(d) \quad \text{(Eq.11)} \\ \text{If } d < k, & NPP_{grain}(d) = 0 \quad \text{(Eq.12)} \end{cases}$$

And finally,

$$grain(d) = \sum_{i \leq d} (NPP_{grain}(i)) \quad \text{(Eq.13)}$$

The variable *grain* (in t DM ha^{-1}) could be considered either as reproductive structures + grain, or grain only. The parameter n_{thresh} is a threshold in the number of leaves from which either the formation of reproductive structures starts, or the grains form or the grain filling starts. Above equations aim to be generic and to reproduce the diversity of approaches in GGCMs. That is why we do not distinguish here the production of reproductive structures and the accumulation of assimilates in grains after anthesis.

Equations 1-7 and 10-13 are called SMM (for Simple Mechanistic Model) in the following. We focused on *biom* and *grain* at maturity, i.e. computed on the last day of the growing season t_m. They are called $biom_{SMM}$ and $grain_{SMM}$ in the following:

$$biom_{SMM} = biom(t_m) \quad \text{(Eq.14)}$$

$$grain_{SMM} = grain(t_m) \quad \text{(Eq.15)}$$

https://doi.org/10.5194/gmd-2020-113
Preprint. Discussion started: 24 June 2020
© Author(s) 2020. CC BY 4.0 License.

Geoscientific Model Development Discussions

The variable $grain_{SMM}$ is used to approach the potential yield. Our analysis focuses on maize because of the importance of cereals in human food and because of the widespread distribution of this crop across latitudes.

175

2.2 Set-up

We focused first on the computation of $biom_{SMM}$, then on the relationship $grain_{SMM}$ vs $biom_{SMM}$. The sensitivity of SMM to each parameter involved in the computation of $biom_{SMM}$ was first studied. 180 Then, we calibrated SMM against each GGCM to make the spatial distribution of $biom_{SMM}$ mimic the spatial distribution of aboveground biomass at maturity simulated by each GGCM (called $biom_{GGCM}$ hereafter). This calibration happened in two steps. The 1st step concerned *C* and *RUE* which have one value at the global scale. The 2nd step concerned GDD_{1leaf} that we made varying in space to mimic procedure used by GGCM modellers in GGCMI (see below). The choice of 185 focusing on *C*, *RUE* and GDD_{1leaf} is justified below. In a last step (step 3), we calibrated n_{thresh} and *frac* to make SMM mimic the relationship *grain* vs *biom* of each GGCM.

2.2.1. GGCMs and GGCMI simulations considered

190 The eight GGCMs considered in our approach were: LPJ-GUESS (Lindeskog et al., 2013; Smith et al., 2001), LPJmL (Bondeau et al., 2007; Waha et al., 2012), CLM-crop (Drewniak et al., 2013), pDSSAT (Elliott et al., 2014; Jones et al., 2003), pAPSIM (Elliott et al., 2014; Keating et al., 2003), CGMS-WOFOST (Boogaard et al., 2014), GEPIC (Williams et al., 1995) (Folberth et al., 2012; Izaurralde et al., 2006; Liu et al., 2007), EPIC-IIASA (Williams et al., 1995) (Izaurralde et al., 195 2006). GGCMs simulations are provided in the framework of the GGCM Intercomparison (GGCMI) and described in (Müller et al., 2019a). Six other GGCMs also participated in GGCMI but were not considered here as necessary output variables (timing and duration of the growing season for EPIC-BOKU, PEPIC, EPIC-TAMU; aboveground biomass for ORCHIDEE-crop) or simulations (for PRYSBI2) were not provided on the data archive of GGCMI.

200

In GCCMI, all GGCMs followed a common protocol and were forced by the same weather datasets. We focused here on the simulations forced by one of them, the AgMERRA dataset (Ruane et al., 2015). We used simulations forced by the AgMERRA dataset as all GGCMs performed these simulations. Three levels of harmonization have been used in GGCM simulations: *default*, *fullharm*, 205 *harmnon*. In *fullharm* simulations, all GGCMs have been forced by the same prescribed begin/end

https://doi.org/10.5194/gmd-2020-113
Preprint. Discussion started: 24 June 2020
© Author(s) 2020. CC BY 4.0 License.


of the growing season which were derived from a combination of two global datasets (MIRCA (Portmann et al., 2010) and SAGE (Sacks et al., 2010), (Elliott et al., 2015)). In *harmnon* simulations, in addition to forced timing and duration of the growing season, all GGCMs experienced no nutrient limitation, through prescribed fertilizer inputs. Besides this harmonization level, two water regimes have been considered: *irrigated* and *non-irrigated*. For our analysis focusing on the simulation of potential yield, we decided to select the configuration (*harmnon* and *irrigated*). This is true for all GGCMs considered, but CGMS-WOFOST. In fact, the *harmnon* simulation was not provided for CGMS-WOFOST but, because i) this model does not consider nutrient limitation, and ii) the growing season was prescribed in the *default* simulation, we assumed that the potential yield could be approached by the (*default* and *irrigated*) simulation.

For EPIC family models (here, GEPIC and EPIC-IIASA), we used a corrected $biom_{GGCM}$ computed as below as it has been noticed that some issues related to the variable *biom* appeared in the outputs available on the GGCMI data archive likely related to the output time-step of specific variables (Folberth, personnal communication, 2019):

$$biom_{GGCM} = grain_{GGCM} / HI_{max} \qquad \text{(Eq.16)}$$

where HI_{max} is the maximum harvest index (no unit), varying in space as function of cultivars. In EPIC, the actual *HI* at harvest only differs to HI_{max} if a drought stress occurs in the reproductive phase. Because this stress was virtually eliminated by sufficient irrigation in the *harmnon* x *irrigated* simulations, the Eq.16 provides the most accurate estimate of aboveground biomass at harvest. Map of cultivar distribution, used as input to the EPIC models (Figure 1 and Table D in (Folberth et al., 2019)), have been considered here to compute the corrected $biom_{GGCM}$.

2.2.2 Input variables for SMM

We focused our analysis on the growing season starting in calendar year 2000 (and potentially finishing in calendar year 2001). SMM was forced by the short-wave downwelling radiation (*rsds* in MJ m^{-2} day^{-1}) and the daily mean temperature (*tas*, in °C) from the AgMERRA weather dataset (Ruane et al., 2015). SMM also needs the begin and end of the maize growing season and we used respectively the planting day (t_p) and the timing of maturity (t_m), both being provided in the output of each GGCM. Despite the fact that all GGCMs are forced by the same growing season in *harmnon*, some GGCMs allow flexibility in regards to t_p and t_m prescribed as input (Müller et al., 2019b), as suggested by the GGCMI protocol: *"crop variety parameters (e.g., required growing degree days to reach maturity, vernalization requirements, photoperiodic sensitivity) should be*

https://doi.org/10.5194/gmd-2020-113
Preprint. Discussion started: 24 June 2020
© Author(s) 2020. CC BY 4.0 License.

Geoscientific Model Development Discussions

adjusted as much as possible to roughly match reported maturity dates". Thus, we cannot use t_p and t_m from GGCM input files (Text S1).

We performed SMM simulations (and thus, computed $biom_{SMM}$ and $grain_{SMM}$) for each GGCM, i.e. for each GGCM growing season. For a given GGCM, SMM simulations were performed only for grid-cells considered in the given GGCM. In addition, grid-cells for which information about the growing season from MIRCA and SAGE was not available are masked to prevent to consider grid-cells where internal GGCM computation was performed.

The maps of cultivar distribution used by EPIC models (Folberth et al., 2019) were also used as inputs to SMM in the simulation aiming to mimic the *biom* vs *grain* relationship of EPIC models (see Sect.2.2.4.2).

2.2.3 Sensitivity of global $biom_{SMM}$ to SMM parameters

Except the active fraction of short wave downward radiation (f in Eq.4) the value of which is physically well-known, other parameters involved in the computation of $biom_{SMM}$ (T_0, max_{nleaf}, GDD_{1leaf}, *C, RUE)* are relatively uncertain. The sensitivity of the global averaged $biom_{SMM}$ to these parameters was assessed by performing 3125 (i.e. 5^5) SMM simulations allowing to combine 5 different values for each parameter. In each of these SMM simulations, a given parameter was constant in space. The initial estimate of each parameter was provided in Table S1. While the initial estimate of each parameter was based on literature, we chose quite arbitrarily the same range of variation of [50-150%] (in % of the initial estimate) for all parameters, with the 5 values tested uniformly distributed within the range of variation (i.e. 50, 75, 100, 125, 150% of initial guess).

Following our current knowledge based on observations, it would be partly possible to choose a different uncertainty range for each parameter: for instance, literature tends to show that *RUE* is relatively well constrained for maize (Sinclair and Muchow, 1999) while the *C* parameter, which depends on plant density, is expected to vary a lot as a function of the farming practices (Sangoi et al., 2002; Testa et al., 2016) (Table S1). However, SMM aimed to mimic GGCMs and not observations, and it is quite difficult to know if parameter values used in GGCMs well reflect our current knowledge. For instance, there is some confusion in values of *RUE* reported in the literature following the diversity of experimental approaches and units of expression that have been used (Sinclair and Muchow, 1999). Some confusion in *RUE* values exists in the literature between *RUE* expressed in g of DM per MJ of intercepted solar radiation (called here *RUE'*) or in g of DM per MJ of intercepted *PAR* (*RUE"*, with *RUE"=RUE'*/0.5) or in g of DM per MJ of absorbed *PAR* (*RUE"'*, with *RUE"'=RUE'*/0.425) (Sinclair and Muchow, 1999) and this could lead to erroneous values in

https://doi.org/10.5194/gmd-2020-113
Preprint. Discussion started: 24 June 2020
© Author(s) 2020. CC BY 4.0 License.

Geoscientific Model Development Discussions

GGCMs. In the following, we used MJ of absorbed *PAR*, to be consistent with our Eq.6. Observations also showed that *RUE* decreases during grain filling following the mobilization of leaf nitrogen to the grain (Sinclair and Muchow, 1999). Thus, *RUE* is larger during vegetative growth (3.8-4.0 g DM (MJ of absorbed PAR) $^{-1}$ (Kiniry et al., 1989)) than averaged over the whole season (3.1-4.0 g DM MJ^{-1} (Sinclair and Muchow, 1999)). It is likely than some GGCMs used *RUE* values which are not representative to the whole growing season. Thus, we used the same range of uncertainty for all parameters in our calibration procedure. Exploring a wider range of values also allows for a more complete assessment of GGCM performance.

Potential confusion in units mentioned above also lead us to chose an initial estimate of *RUE* (2 g DM MJ^{-1}) lower than values commonly reported in the literature (3.1-4.0 g DM MJ^{-1}) (Sinclair and Muchow, 1999) but note that the highest values of *RUE* tested during our calibration (3.0 g DM MJ^{-1}) reach the literature-based range.

The global mismatch between each GGCM and SMM was quantified thanks to the Root Mean Square Error (RMSE) computed as follows:

$$RMSE(u)=\sqrt{\frac{1}{N}\sum_{g=1}^{N}(biom_{SMM}(u,g)-biom_{GGCM}(g))^2} \quad \text{(Eq.17)}$$

where u is a combination of parameters and g is a grid-cell among the N grid-cells considered for each GGCM. All grid-cells are assumed independent and have the same weight in the RMSE computation. RMSE has the same unit as *biom* (t DM ha^{-1}).

2.2.4 SMM calibration against each GGCM

SMM was calibrated following 3 steps. The first two steps aimed to mimic $biom_{GGCM}$ distribution while the last step aimed to make SMM reproduce the relationship *grain* vs *biom* of each GGCM. The procedure of calibration was summarized in Table 2. "*Emulated GGCM*" is used from now to define SMM output after SMM calibration aiming to mimic a given GGCM.

2.2.4.1 Parameters involved in the computation of $biom_{SMM}$

Regarding the simulation of *biom*, we restricted the calibration to *RUE*, *C* and GDD_{1leaf} as follows: f is well constrained, max_{nleaf} has a small effect on global simulated $biom_{SMM}$ (see below the results of the analysis prescribed in Sect.2.2.3), T_0 co-varies with GDD_{1leaf} and we decided to focus on

https://doi.org/10.5194/gmd-2020-113
Preprint. Discussion started: 24 June 2020
© Author(s) 2020. CC BY 4.0 License.

GDD_{1leaf} (see below). These parameters (f, max_{nleaf}, T_0) were prescribed equal to their initial estimate and were the same for all SMM simulations.

We choose to make C and RUE globally constant and GGCM-dependent. The decision to not make C and RUE vary in space is consistent with the rule of parsimony, that we aimed with SMM. It also follows the procedure commonly used in GGCMs that involved similar approach. For instance, GEPIC is based on a biomass-energy conversion coefficient that does not vary in space (Folberth et al., 2016). Plant density (hidden in C) is constant in space in LPJmL (Schaphoff et al., 2018b). We calibrated C and RUE at the same time to assess potential compensation between these parameters in SMM. The three pairs (C, RUE) that minimized the most the global RSME computed following Eq.17 among the pairs tested were chosen. A fourth pair corresponding to (C, RUE), where C is equal to its initial estimate, has been used. The use of four different pairs aimed to assess the sensitivity of our conclusions to the parameter values. For each (C, RUE) pair, we finally calibrated GDD_{1leaf}. We made GDD_{1leaf} vary in space as it it is allowed in the GGCMI exercise. In the GGCMI protocol, accumulated thermal requirements were adjusted to catch the growing season (duration and timing) prescribed as input in the *harmnon* GGCM simulation. In SMM, the procedure slightly differs as we calibrated thermal requirements to match $biom_{GGCM}$: for each grid-cell, GDD_{1leaf} is chosen among its 5 possible values to minimize the absolute difference between $biom_{GGCM}$ and $biom_{SMM}$. Grid-cells were considered independently.

The ability of SMM to match the spatial distribution of $biom_{GGCM}$ for each GGCM after SMM calibration was measured through: the bias, RMSE and Nash-Sutcliffe model efficiency coefficient (NS) defined as:

$$NS = 1 - \frac{\sum_{g=1}^{N} (biom_{SMM}(g) - biom_{GGCM}(g))^2}{\sum_{g=1}^{N} (biom_{GGCM}(g) - \overline{biom_{GGCM}})^2} \quad \text{(Eq.18)}$$

where g refers to any grid-cell and $\overline{biom_{GGCM}}$ is the average of $biom_{GGCM}$ over grid-cells. NS=1 means that SMM perfectly matches the spatial distribution of $biom_{GGCM}$.

To assess the mismatch between $biom_{GGCM}$ and $biom_{SMM}$ after SMM calibration for a given GGCM, we compared the RMSE of two sub-groups of grid-cells that differ according to a third variable related to climate or soil type.

https://doi.org/10.5194/gmd-2020-113
Preprint. Discussion started: 24 June 2020
© Author(s) 2020. CC BY 4.0 License.

2.2.4.2 Parameters involved in the computation of $grain_{SMM}$

C, *RUE* and GDD_{1leaf} determine *biom* simulated by SMM at each time-step. Two SMM parameters are involved in the computation of *grain* for any day from *biom*, namely n_{thresh} and *frac*. The calibration of these parameters aims to make SMM able to mimic the relationship between *grain* and *biom* at the end of the growing season from each GGCM. One global and GGCM-dependent pair (n_{thresh}, *frac*) was chosen by using the following criteria:

$$\begin{cases} \text{if } A_{GGCM}=0, \text{ find } u \text{ that minimizes } \quad R_{slope}(u)=\left|a_{GGCM}-a_{SMM}(u)\right| & \text{(Eq.19)} \\ \text{if } A_{GGCM}\neq 0, \text{ find } u \text{ that maximizes } \quad R_{areas}(u)=\left(\frac{A_{GGCM}\cap A_{SMM}(u)}{max\left(A_{GGCM},A_{SMM}(u)\right)}\right) & \text{(Eq.20)} \end{cases}$$

where *u* corresponds to a given pair (n_{thresh} , *frac*), A_X is the area defined by the grid-cell clouds in the *grain* vs *biom* space for *X*, a_X is the slope of the linear regression $grain_X \sim biom_X$, with *X* in {GGCM, SMM}.

In other words, if $grain_{GGCM}$ vs $biom_{GGCM}$ is a line, (n_{thresh} , *frac*) is chosen to make the relationship between $grain_{SMM}$ vs $biom_{SMM}$ linear with the same slope as the one of the GGCM. If $grain_{GGCM}$ vs $biom_{GGCM}$ is not a line, the grid-cells in the space $grain_{GGCM}$ vs $biom_{GGCM}$ define an non-null area, called A_{GGCM} and (n_{thresh} , *frac*) is chosen to make A_{SMM} as similar as possible to A_{GGCM}. EPIC family GGCMs introduced a cultivar diversity in parameters related to grain filling and in that case, the calibration of (n_{thresh}, *frac*), instead of being done at the global scale, was made for each cluster of grid-cells corresponding to a given cultivar. The distribution of cultivars from EPIC was used as input of SMM in that case.

2.3 Contribution of different processes to yield in SMM

We computed ratios between some SMM internal variables to assess the global contribution of different processes represented in SMM to the achievement of $grain_{SMM}$. The following ratios have been computed: n_{leaf}/tas, $APAR/rsds$, $APAR/n_{leaf}$, $biom/APAR$, $grain/biom$. The ratio n_{leaf}/tas represents the phenology sensitivity to temperature; $APAR/rsds$ reflects how radiation is absorbed by the canopy and $APAR/n_{leaf}$ represents the absorption sensitivity to phenology, $biom/APAR$ reflects the conversion from absorbed radiation to biomass and $grain/biom$ represents the harvest index.

We also investigated how the contribution of the different processes to the achievement of $grain_{SMM}$ varies between emulated GGCMs. Variations in these ratios reflects the difference in global

https://doi.org/10.5194/gmd-2020-113
Preprint. Discussion started: 24 June 2020
© Author(s) 2020. CC BY 4.0 License.

averaged key parameters between emulated GGCMs. For instance, variations in *grain/biom* between emulated GGCMs reflects differences in calibrated n_{thresh} and *frac* (Fig.S3).

To compute the different ratios, averages over the growing season were used for *tas*, *rsds*, *APAR* and n_{leaf}, while the end of the growing season were used for *biom* and *grain* (so called $biom_{SMM}$ and $grain_{SMM}$, Eq. 14-15). A given ratio was computed for each grid-cell and its grid-cell distribution was plotted in the following as barplot (Sect.3.4 and Fig.8).

https://doi.org/10.5194/gmd-2020-113
Preprint. Discussion started: 24 June 2020
© Author(s) 2020. CC BY 4.0 License.

Geoscientific Model Development Discussions

3. Results

3.1 Global averaged $biom_{SMM}$: sensitivity to each parameter and calibration of (*C*, *RUE*)

As expected when looking at Eq.6-7, the global averaged $biom_{SMM}$ sensitivity to *RUE* was large (Fig.2). Varying *RUE* was the only way possible to capture the global averaged $biom_{GGCM}$ for LPJ-GUESS (Fig.2). The global averaged $biom_{SMM}$ was only slightly sensitive to other parameters as compared to the sensitivity to *RUE*. When all parameters are equal to their initial estimate, *RUE* minimizing the RMSE computed following Eq.17 was: 1.0 (LPJ-GUESS), 2.0 (LPJmL), 1.5 (CLM-crop), 2.5 (pDSSAT), 1.5 (pAPSIM), 2.0 (CGMS-WOFOST), 1.5 (GEPIC), 1.5 g DM MJ^{-1} (EPIC-IIASA).

In Fig.3, we plotted how RMSE changes according to both *C* and *RUE* varying at the same time, all other parameters being equal to their initial estimate. Figure 3 shows that *C* and *RUE* can compensate in SMM. Calibrating (*C*, *RUE*) (with one global value for each parameter) allows to reach RMSE around 4 t DM ha^{-1} for all GGCMs but LPJ-GUESS and LPJmL (around 2 and 3 t DM ha^{-1} respectively) (Fig.3). We chose 3 pairs (*C*, *RUE*) among the 25 tested couples that minimized the RMSE to assess the sensitivity of our conclusions to the pair chosen. Using a fourth pair with the same *C* for all GGCMs equal to its initial estimate decreased only slightly the ability of SMM to match the GGCMs (magenta dots in Fig.3) and did not change drastically the *RUE* compared to the ones when both *C* and *RUE* were calibrated.

3.2 Calibration of GDD_{1leaf}

Once (*C, RUE*) was globally chosen, a spatially varying GDD_{1leaf} was calibrated. After calibration, SMM was able to catch the spatial variability of $biom_{GGCM}$ for most GGCMs (Fig.4 and Fig.5a). Difference in percent can be large, especially for regions with small *biom* but the global distribution was relatively well captured (Fig.4).

Global RMSE reaches between ~1 (LPJ-GUESS) and 3.3 t DM ha^{-1} (EPIC-IIASA) (Fig.5a). The Nash-Sutcliffe coefficient (NS) is large (≥0.6) for all GGCMs but CLM-crop (0.46) and pAPSIM (0.41). RMSE is greater if computed for grid-cells that experience some days with temperature above 30°C than if computed for grid-cells without such days, for LPJ-GUESS (1.5 t DM ha^{-1} vs 0.8), GEPIC (4.4 vs 2.3), EPIC-IIASA (4.2 vs 2.8) and pAPSIM (3.5 vs 2.3) (not shown). Nevertheless, the implementation of a heat stress within SMM (TextS S2) increases only slightly the fit of SMM vs GGCM for these GGCMs: e.g. NS increases from 0.41 (without heat stress) to

https://doi.org/10.5194/gmd-2020-113
Preprint. Discussion started: 24 June 2020
© Author(s) 2020. CC BY 4.0 License.

Geoscientific Model Development Discussions

0.52 (with heat stress) for pAPSIM (Fig.S5). The limited increase can be explained by the fact that optimized GDD_{1leaf} in the SMM simulation without heat stress encompasses a part of the heat stress for these grid-cells.

EPIC family GGCMs simulate some other stresses, such as stresses related to salinity and aeration, that could have an effect on the potential yield even in the (*harmnon* and *irrigated*) simulations (Müller et al., 2019a). The intensity of some of these stresses (aeration) depends on soil orders and should be particularly important in vertisols (C.Folberth, personal communication, 2019). However, RMSE is only slightly different for grid-cells characterized by vertisols vs others soil orders for GEPIC (3.4 for vertisols vs 3.2 for other soil orders) and EPIC-IIASA (3.8 vs 3.3).

CLM-crop (NS=0.46) and pAPSIM (NS=0.52 for SMM configuration with heat stress) are the two GGCMs for which the GGCM vs SMM agreement remains relatively poor.

When using other (*C, RUE*) pairs, the fit SMM vs GGCM overall slightly decreases for most GGCMs as the (*C, RUE*) chosen tends to lower global fit when GDD_{1leaf} is constant (see RMSE for the different pairs given in Fig.3) but same conclusions as above are reached: the fit are relatively correct, except for CLM-crop and pAPSIM (Fig.S6). Calibrating GDD_{1leaf} when the 4th (*C*, *RUE*) pair is used leads to reasonable fit between SMM and GGCM (Fig.5b): calibrating *C* is of second order as compared to calibration of *RUE*.

The distribution of calibrated GDD_{1leaf} is provided in Fig.6. This distribution varies between GGCMs. Most of the grid-cells are characterized by extreme GDD_{1leaf} values. The distribution of GDD_{1leaf} is also sensitive to the chosen (*C*, *RUE*) pair, in particular for LPJ-GUESS and LPJmL. For these GGCMs, the difference ($biom_{GGCM}$ – $biom_{SMM}$) is small and has the same sign almost everywhere (Fig.4, last column). The sign is sensitive to the chosen (*C, RUE*): for instance, the difference is negative for the 1st (*C, RUE*) pair and positive for the 2nd one for LPJ-GUESS. The calibration of GDD_{1leaf}, as it happens after the calibration of (*C, RUE*), tends to compensate this systematic bias and varies between pairs.

A SMM simulation where the range of variation allowed for GDD_{1leaf} during the step 2 of the calibration is increased (from [50-150%] * initial estimate in default calibration to [25-200%] * initial estimate) allows to significantly improve the match GGCM vs SMM: NS coefficient increases for CLM-CROP (from 0.46 to 0.66) and pAPSIM (from 0.41 to 0.60) (2nd line of Fig.S7). Increasing the sensitivity to temperature by letting both GDD_{1leaf} and T_0 vary at the same time

https://doi.org/10.5194/gmd-2020-113
Preprint. Discussion started: 24 June 2020
© Author(s) 2020. CC BY 4.0 License.


during the calibration give similar results (3rd line of Fig.S7). These results are obvious as allowing more variation in SMM allows a best fit to GGCM in more grid-cells. This underlines the difficulty to make SMM functioning as a mechanistic model (see Discussion).

3.3 Calibration of parameters involved in grain computation (n_{thresh}, *frac*)

Varying (n_{thresh}, *frac*) allows the dots (corresponding to the different grid-cells) to define different shapes in the space $yield_{SMM}$ vs $biom_{SMM}$ (Fig.S8 for pDSSAT as example). n_{thresh}=0 leads to linear relationship between $yield_{SMM}$ and $biom_{SMM}$ with a slope equal to *frac* (left panels of Fig.S8). Non-null n_{thresh} make some grid-cells deviate to this linear relationship and the number of such grid-cells increases with n_{thresh} (Fig.S8). For all GGCMs, we found a (n_{thresh}, *frac*) combination that allows the relationship $yield_{SMM}$ vs $biom_{SMM}$ to fit the relationship $yield_{GGCM}$ vs $biom_{GGCM}$ (Fig.7). For CLM-crop, we are not able to reproduce the cloud of dots corresponding to grid-cells where the potential yield is below the line *grain=80%*biom*. For EPIC family GGCMs, a calibration per cluster of grid-cells sharing the same cultivar is required.

3.4 Contribution of different processes to the achievement of $grain_{SMM}$

The ratio n_{leaf}/*tas* is relatively constant among the emulated GGCMs and this is true whatever the (*C, RUE*) pair chosen (Fig.8a). The ratio n_{leaf}/*tas* reflects GDD_{1leaf}. The calibrated GDD_{1leaf}, even if its spatial distribution varies from one GGCM to the other (see previous section), remains relatively constant at the global scale between GGCMs.

The ratios *APAR/rsds* and *APAR*/n_{leaf} (Fig.8b-c) vary a lot between GGCMs but this variation is of the same order of magnitude as the one between (*C, RUE*) pairs. These ratios reflect *C*, which is highly variable between GGCMs and between pairs.

The ratio *biom/APAR* (Fig.8d) reflects global *RUE*. Calibrated *RUE* varies a lot between GGCMs and only slightly between pairs for a given GGCM.

The ratio *grain*/*biom* (Fig.8e) varies a lot between GGCMs and is only slightly sensitive to the (*C, RUE*) pair. This ratio reflects a combination of n_{thresh} and *frac*. GGCMs with n_{thresh} equal to 0 (LPJmL, EPIC-IIASA) have no grid-cell variability in *grain/biom* (Fig.8e). Overall, and whatever the GGCM variability at grid-cell scale, we can distinguish i) emulated GGCMs that convert a large fraction of *biom* to *grain*, as CLM-crop, ii) emulated GGCMs that convert around 50% of *biom* to *grain*, as LPJmL, pDSSAT, GEPIC, pAPSIM, EPIC-IIASA and iii) emulated GGCMs that convert around 30-40% of *biom* to *grain* as LPJ-GUESS and CGMS-WOFOST. Large variation of

https://doi.org/10.5194/gmd-2020-113
Preprint. Discussion started: 24 June 2020
© Author(s) 2020. CC BY 4.0 License.

Geoscientific Model Development Discussions

grain/biom between GGCMs is consistent with the fact that difference in *grain* among GGCMs is larger than the one in *biom* (Fig.1).

https://doi.org/10.5194/gmd-2020-113
Preprint. Discussion started: 24 June 2020
© Author(s) 2020. CC BY 4.0 License.

4. Discussion & Conclusions

We showed that a simple set of equations with one GGCM-dependent global *RUE* and spatially variable thermal requirement (GDD_{1leaf}) is able to mimic spatial distribution of aboveground biomass of most GGCMs. Calibrating one additional global parameter at the same time as *RUE* (namely *C*) improves only slightly the fit between SMM and GGCM and modified in a small extent the calibrated value of *RUE*. *RUE* represents canopy photosynthesis and GDD_{1leaf} determines crop duration, i.e. the two main drivers of crop productivity (Sinclair and Muchow, 1999). The relationship between potential yield and aboveground biomass of GGCM is captured by the calibration of two additional global parameters: one that triggers the start of grain filling and one corresponding to a time-invariant fraction of NPP allocated to the grain. These two parameters allow to catch the relationship between *biom* and *grain* from all GGCMS. This feature of SMM is particularly important as we showed that the divergence between GGCMs is larger for *grain* than for *biom* (Fig.1). Cultivar diversity regarding these latter parameters is nevertheless required to catch the behavior of some GGCMs. Despite apparent complexity in GGCMs, we showed that differences between them in regards to potential yield can be explained by differences in few key parameters.

Our approach has few caveats. First, SMM could be able to fit individual GGCMs for the wrong reasons, i.e. following a compensation between SMM internal processes which is not representative of the considered GGCM. We think that this issue is nevertheless minimized in our approach. First, we investigated how parameters can compensate, e.g. by calibrating at the same time *RUE* and *C*. We showed that calibration of *C* is of second order importance and getting calibrated *RUE* less varying among emulated GGCMs would require very extreme values for *C*, well behind the range of values allowed in our calibration. The parameter *C* encompasses different parameters (see Eq.8) and a better alternative would be to separate them as well as to explicitly simulate the Leaf Area Index (*LAI*) variable. SMM-simulated *LAI* would be compared to GGCM output and this comparison would reduce further the risk of compensation between processes in SMM. However, *LAI* was not available neither from GGCMI data archive nor upon request to GGCM modellers. We stress the need to incorporate this output variable in next inter-comparison exercise. It is also important to note that the average over the growing season of *LAI* or *LAI* at set fractions of the growing season (including anthesis) would be more interesting than *LAI* at harvest as, under potential conditions, *LAI* at harvest is very likely close to maximum *LAI* allowed by the different GGCMs.

https://doi.org/10.5194/gmd-2020-113
Preprint. Discussion started: 24 June 2020
© Author(s) 2020. CC BY 4.0 License.

Geoscientific Model Development Discussions
Open Access
EGU

Then, the reasonable match between SMM-simulated aboveground biomass and GGCM-simulated *biom* is made possible only because of the large range of variation allowed for *RUE* and GDD_{1leaf} during the calibration, i.e. [50,150%] of their initial estimate. This range should have a meaning in term of values commonly used in GGCMs. Otherwise, the calibrated parameters could implicitly encompass different mechanisms considered in GGCMs but not in SMM and this issue should occur more likely as we choose a large range of variations. For instance, calibrated GDD_{1leaf} in SMM could artificially encompass the sensitivity to temperature of processes not considered in SMM, as we discussed for heat stress in Sect.3.2. It is likely that the variation of GDD_{1leaf} also encompasses a spatial variation of emergence in GGCMs as in SMM, we did not compute emergence and plants starts to grow from the planting day. In such cases, SMM should not be considered as a pure mechanistic model but more as a meta-model and, purely statistical meta-models should be more appropriate than our simplified process-based model. However, the range of variation that we used for GDD_{1leaf} ([50-150%] around the initial estimate of 43°C, corresponding to ~[22-65°C]) is consistent with ranges reported by observations focusing on the sensitivity of phyllochron (thermal requirement for the emergence of any leaf) to temperature (Fig.2 of (Birch et al., 1998)) and cultivar (Padilla and Otegui, 2005). Our range of GDD_{1leaf} cannot be straightforward compared to the range of heat unit commonly used in GGCMs to catch the prescribed growing season (e.g. ~[10-225°C] in GEPIC if we divide the values of heat units given in (Minoli et al., 2019) by a maximum number of leaves of 19, as in our study) or computed in (van Bussel et al., 2015a) (~[25-160°C] if we divide the values given in Fig.2 of that reference by 19). Indeed, in our approach, $GDD_{1leaf}*max_{nleaf}$ correspond to the thermal requirement up to the emergence of all leaves while the sum of heat unit used in GEPIC or (van Bussel et al., 2015a) is required to reach the maturity and thus encompasses both the emergence of all leaves and the period from flowering (concomitant to the end of leaves emergence) up to maturity.

Some discrepancies remain between SMM and some GGCMs, especially CLM-crop and pAPSIM. This could be explained by differences between GGCM and SMM in the choice of processes represented (e.g. net productivity in SMM instead of balance between gross productivity and plant respiration in some GGCMs) or for a given process, in the choice of equations used to represent it (e.g. Farquhar (CLM-crop) vs *RUE* (SMM) for assimilation). The representation of stomatal conductance and CO_2 assimilation rate within Farquhar equations introduces a sensitivity to variables not considered in the *RUE*-based approach (e.g. water vapour pressure deficit) in line with observations that show that *RUE* is sensitive to many variables (Sinclair and Muchow, 1999). This would lead to differences in the spatial variability of simulated aboveground biomass as compared

https://doi.org/10.5194/gmd-2020-113
Preprint. Discussion started: 24 June 2020
© Author(s) 2020. CC BY 4.0 License.


to one simulated with spatially constant *RUE*. The succession of phenological stages with different parametrizations in some GGCMs (e.g. in pAPSIM (Wang et al., 2002)) can also partly contribute to differences with SMM as plant development is continuously simulated in SMM, as it is in other GGCMs (e.g. LPJmL, (Schaphoff et al., 2018a)). Other possibility of mismatch is related to some limiting factors (nutrients, water, etc.) that could exist in the *harmnon* and *irrigated* simulation for GGCMs despite the protocol of these simulations and through different biases. First, GGCMs that do not explicitly simulate nutrient limitations may have integrated these stresses implicitly in their parametrizations (see next paragraph). Second, irrigation in some GGCMs ensures that plants are not limited by water supply. But plants can still experience water stress if the atmospheric demand is higher than the plant hydraulic structure can service. This could likely explain the lower yield for the group of grid-cells below the line corresponding to $grain_{GGCM}$=80%*$biom_{GGCM}$ for CLM-Crop in Fig.7. Finally, some other stresses (salinity, aeration, etc.) are present in few GGCMs (e.g. EPIC family models) and are not alleviated in *harmnon* simulation. However, it seems that these stresses, restricted to few grid-cells, cannot significantly contribute to the GGCM vs SMM mismatch.

Despite some confusion in values of *RUE* reported in the literature arising from diversity of experimental approaches and units of expression that have been used ((Sinclair and Muchow, 1999); Sect.2.2.3), *RUE* is relatively well constrained from observations ([3.1-4.0] g DM MJ^{-1}). Here, we found that calibrated *RUE* in emulated GGCMs are lower than values derived from observations and varied a lot among GGCMs: between 1 for LPJ-GUESS to 2.5 g DM MJ^{-1} for pDSSAT. The values of calibrated *RUE* found in our study can be compared to values actually used in GGCMs based on the same approach of conversion of radiation to aboveground biomass. *RUE* used in GEPIC is equal to 4.0 g DM MJ^{-1} (C.Folberth, personal communication, 2020) while our calibrated value for the same GGCM is of 2.0 g DM MJ^{-1}. Our calibrated *RUE* is an apparent *RUE* and the mismatch with actual *RUE* prescribed to GEPIC can be explained as follows. First, the daily increment of biomass in GEPIC derived from the conversion of radiation encompasses an increment for both aboveground biomass and roots (with a ratio root:total varying from 0.4 at germination to 0.2 at maturity) while both the *RUE* values used in SMM and derived from most observations (Sinclair and Muchow, 1999) concern aboveground biomass only. Second, LAI_{max} in GEPIC is lower than values used in SMM: in GEPIC, LAI_{max} which vary with plant density and is equal to 3.5 at plant density of 5 used in these simulations while LAI_{max} in SMM (derived from Eq.9 when n_{leaf} reaches its maximum) is equal to 5. Lower LAI_{max} in GEPIC than SMM can compensate higher *RUE*. Finally, the seasonal dynamic of *LAI* could be different between GEPIC and SMM and this can counter-balance the lower increment of biomass computed in SMM than in GEPIC once LAI_{max}

https://doi.org/10.5194/gmd-2020-113
Preprint. Discussion started: 24 June 2020
© Author(s) 2020. CC BY 4.0 License.


is reached. As mentioned above, the values of *LAI* computed by GGCMs at different set fractions of the growing season would be very helpful.

The diversity in apparent *RUE* found between GGCMs raises the question about the physical meaning of the parameters used in each GGCM. GGCMs are tools first dedicated to simulate actual yield and could have been tuned in that purpose against local observations. During that tuning, processes not explicitly represented in a given GGCM could be implicitly incorporated in parametrizations of other processes. For instance, it could be the case for GGCMS that do not incorporate explicitly nutrient limitations. Potential yield is a variable that has been computed in a second step and that could suffer from these implicit incorporations. At the end, the divergence in potential yield between GGCMs raise the questions about their ability to reproduce real process at the basis of actual yield as this latter depends on the combination between potential yield and many limiting factors.

Our study has some implications for GGCMs modellers in regards to the simulation of potential yield. We showed that differences between GGCMs can be explained by differences in few key parameters, namely the *RUE* and parameters driving the grain filling (n_{thres} and *frac*). For *RUE*, we recommend to GGCMs modellers to investigate why each individual GGCM has a so small (explicit or implicit) apparent *RUE*. We showed that n_{thresh} and *frac* vary a lot between GGCMs. For GGCMs with n_{thresh} equal to 0, a parametrization based on a better distinction between emergence of all leaves and the period from flowering to maturity could be interesting. We also showed that n_{thresh} and *frac* determines harvest index (*HI*) and we showed that *HI* vary a lot between GGCMs. Thus, we advice that more effort needs to be directed in assembling a global dataset of *HI* for either parametrization or evaluation of GGCMs. Maximum *HI* that plant can reach is a cultivar characteristic and one possibility to build such dataset could partly rely on information from seed companies. Finally, we suggested that next inter-comparison exercise encompass *LAI* and the begin-end of the different growing season periods (vegetative period, flowering, etc.) for GGCMs that distinguish such stages.

Model ensemble mean or median from inter-comparison exercise is commonly preferred to individual GGCM as it has better skill in reproducing the observations (Asseng et al., 2014; Martre et al., 2015). Our mechanistic-model tuned against GGCMs could be a viable alternative to this ensemble mean/median as it allows to keep tracks of processes leading to the final variable, namely here the potential yield. Once tuned, SMM could be forced by an ensemble of parameters to reproduce the ensemble of GGCMs. Our emulator could also offer a potential for GGCMs

https://doi.org/10.5194/gmd-2020-113
Preprint. Discussion started: 24 June 2020
© Author(s) 2020. CC BY 4.0 License.


evaluation and analysis of their structural uncertainty. Its use under different climate and CO_2 conditions would nevertheless require the implementation of some missing mechanisms (e.g. heat stress and effect of CO_2).

In purpose to simulate potential yield at the global scale, our emulator forced by daily temperature and radiation, growing season and with few adjustable parameters could be considered as an interesting alternative to GGCMs as they are easier to manipulate and allow much faster simulations. For instance, our model could be used to investigate the implementation of cultivar diversity at the global scale. The introduction of cultivar diversity is a keystone in development of crop models at the global scale (Boote et al., 2013). Cultivar diversity considered at the global scale was mainly related to phenological development through sensitivity to photoperiod, sensitivity to temperature (and vernalization for winter cultivars) (van Bussel et al., 2015b). The effect of cultivar diversity on allometry (e.g. through variability in harvest index) was considered in a less extensive extent at the global scale and restricted to some EPIC models (Folberth et al., 2019) or pDSSAT in a specific study (Gbegbelegbe et al., 2017). Through protocol of GGCMI in which thermal requirements are tuned to match the growing season, a cultivar diversity was implicitly accounted for. The same applies for SMM. The parameters of the emulator, here fitted to reproduce GGCM output could also be fitted to global dataset based on census/observations in a manner similar to that done with PEGASUS (Deryng et al., 2011) but here applied on potential yield (against real yield for PEGASUS). For instance, SMM could be calibrated against global dataset of potential yield based on statistical approach (Mueller et al., 2012) and the spatial variation of calibrated parameters could be compared to existing knowledge about the spatial distribution of cultivars. Finally, our model because it allows temporal dynamic simulation could be coupled with simulation of limiting factors (water, nutrients) to investigate the limitation of potential yield at the global scale in a simple but mechanistic manner.

https://doi.org/10.5194/gmd-2020-113
Preprint. Discussion started: 24 June 2020
© Author(s) 2020. CC BY 4.0 License.

Data and Code availability

Scripts at the basis of this study are made available on this link:
https://doi.org/10.15454/9EIJWU

They encompass three python scripts and shell scripts + directories to use these python scripts. First python script (called SIM.Py) encompasses SMM equations and performs SMM simulations for different combinations of parameters and for each GGCM growing season. Second one (ReadMultiparam_WriteOPTIM.py) performs the SMM calibration against each GGCM output. Third one (ReadPlotOPTIM.py) performs the main plots. GGCM inputs and outputs required to force or calibrate SMM are available following (Müller et al., 2019a).

Author Contribution

B.R conceived the project, wrote the different scripts and performed the 1st analysis of the results; C.M, T.A.M.P, C.F provided their expertise on the GGCM outputs; all co-authors participated to the analysis of the results and to the writing.

Competing interests

The authors declare no conflict of interest.

Acknowledgements

This research was supported by INRAE (Institut National de Recherche pour l'Agriculture, l'alimentation et l'envrionnement) and the AgroEnv division trough the funding of a "Pari Scientifique 2020". We thank: David Vidal and Lionel Jordan-Meille for discussions at the basis of the simple mechanistic model developed, Marko Kvakić for helpful discussions at the beginning of this study and Mark Irvine for help with the computing aspects. Modelling and analysis were performed in using Python (Python Software Foundation. Python Language Reference, version 2.7. Available at http://www.python.org).

https://doi.org/10.5194/gmd-2020-113
Preprint. Discussion started: 24 June 2020
© Author(s) 2020. CC BY 4.0 License.

Geoscientific Model Development Discussions

Tables

Table 1. List of variables and parameters in SMM.

	Definition	Unit	Status
tas	Daily mean temperature	°C	Input variable
TT	Thermal time	°C	Internal variable
GDD	Sum of growing degree days	°C	Internal variable
n_{leaf}	Number of leaves per plant	-	Internal variable
rsds	Short wave downward radiation	MJ m^{-2} day^{-1}	Input variable
PAR_{inc}	Incoming Photosynthetic Active Radiation	MJ m^{-2} day^{-1}	Internal variable
APAR	Canopy absorbed incoming PAR	MJ m^{-2} day^{-1}	Internal variable
NPP_{biom}	Net primary productivity dedicated to aboveground biomass	g DM m^{-2} day^{-1}	Internal variable
biom	Aboveground biomass	g DM m^{-2}	Internal variable. The study focuses on *biom* at the end of the growing season, called $biom_{SMM}$, and converted in tDM ha^{-1}
NPP_{grain}	Net primary productivity dedicated to grains	g DM m^{-2} day^{-1}	Internal variable
grain	Grain biomass (yield)	g DM m^{-2}	Internal variable. The study focuses on *grain* at the end of the growing season, called $grain_{SMM}$., and converted in tDM ha^{-1}
T_0	Zero of vegetation	°C	Parameter
GDD_{1leaf}	Sum of growing degree day required for each leaf (phyllochron)	°C	Parameter
max_{nleaf}	Maximum number of leaves per plant	-	Parameter
f	Active fraction of short wave downward radiation	-	Fixed parameter (f=0.48)
C	$C=k*S_{leaf}*d_{plant}$ with k: coefficient of extinction of radiation in canopy, S_{leaf}: the specific leaf area of any leaf and d_{plant}: the plant density	-	Parameter
RUE	Radiation Use Efficiency	g DM MJ^{-1} (Here, MJ refers to absorbed *PAR*)	Parameter

https://doi.org/10.5194/gmd-2020-113
Preprint. Discussion started: 24 June 2020
© Author(s) 2020. CC BY 4.0 License.

Geoscientific Model Development Discussions
Open Access
EGU

n_{thresh}	Number of leaves from which either the formation of reproductive structures starts, or the grains form or the grain filling start	-	Parameter
frac	Fraction of NPP_{biom} going towards the variable *grain* when $n>n_{thresh}$	-	Parameter

Table 2. Strategy of SMM calibration for each parameter

Step of calibration	Parameters	Values used in SMM simulations	GGCM variable used for the calibration
	f, T_0, max_{nleaf}	One value at the global scale and same for all GGCMs	None
1	*C*, *RUE*	One value at the global scale and GGCM-dependent	Global averaged *biom*
3	n_{thresh}, *frac**		Relationship *grain* vs *biom*
2	GDD_{1leaf}	Variable in space and GGCM-dependent variability	Spatial variability of *biom*

*: n_{thres} and *frac* are variable in space as function of the cultivar when SMM aims to mimic EPIC family models as these latter consider some cultivar diversity in harvest index.

https://doi.org/10.5194/gmd-2020-113
Preprint. Discussion started: 24 June 2020
© Author(s) 2020. CC BY 4.0 License.

Geoscientific Model Development Discussions
Open Access
EGU

Supplementary Information

https://doi.org/10.5194/gmd-2020-113
Preprint. Discussion started: 24 June 2020
© Author(s) 2020. CC BY 4.0 License.

References

Boogaard, H. L., Wit, A. J. W. D., Roller, J. A. T. & Diepen, C. A. V. WOFOST Control Centre 2.1 and WOFOST 7.1.7. User's guide for the WOFOST Control Centre 2.1 and WOFOST 7.1.7 crop growth simulation model. (Alterra, Wageningen University & Research Centre, Wageningen, The Netherlands, 2014)

Williams, J. R. In Computer models of watershed hydrology (Singh, V. P. ed.) 909–1000 (Water Resources Publications, 1995)

Asseng, S., Ewert, F., Martre, P., Rötter, R. P., Lobell, D. B., Cammarano, D., Kimball, B. A., Ottman, M. J., Wall, G. W., White, J. W., Reynolds, M. P., Alderman, P. D., Prasad, P. V. V., Aggarwal, P. K., Anothai, J., Basso, B., Biernath, C., Challinor, A. J., De Sanctis, G., Doltra, J., Fereres, E., Garcia-Vila, M., Gayler, S., Hoogenboom, G., Hunt, L. A., Izaurralde, R. C., Jabloun, M., Jones, C. D., Kersebaum, K. C., Koehler, A.-K., Müller, C., Naresh Kumar, S., Nendel, C., O'Leary, G., Olesen, J. E., Palosuo, T., Priesack, E., Eyshi Rezaei, E., Ruane, A. C., Semenov, M. A., Shcherbak, I., Stöckle, C., Stratonovitch, P., Streck, T., Supit, I., Tao, F., Thorburn, P. J., Waha, K., Wang, E., Wallach, D., Wolf, J., Zhao, Z. and Zhu, Y.: Rising temperatures reduce global wheat production, Nat. Clim. Change, 5(2), 143–147, doi:10.1038/nclimate2470, 2014.

Birch, C. J., Vos, J., Kiniry, J., Bos, H. J. and Elings, A.: Phyllochron responds to acclimation to temperature and irradiance in maize, Field Crops Res., 59(3), 187–200, doi:10.1016/S0378-4290(98)00120-8, 1998.

Bondeau, A., Smith, P. C., Zaehle, S., Schaphoff, S., Lucht, W., Cramer, W., Gerten, D., Lotze-Campen, H., MüLler, C., Reichstein, M. and Smith, B.: Modelling the role of agriculture for the 20th century global terrestrial carbon balance, Glob. Change Biol., 13(3), 679–706, doi:10.1111/j.1365-2486.2006.01305.x, 2007.

Boogaard, H. L., Wit, A. J. W. D., Roller, J. A. T. & Diepen, C. A. V. WOFOST Control Centre 2.1 and WOFOST 7.1.7. User's guide for the WOFOST Control Centre 2.1 and WOFOST 7.1.7 crop growth simulation model. (Alterra, Wageningen University & Research Centre, Wageningen, The Netherlands, 2014)

Boote, K. J., Jones, J. W., White, J. W., Asseng, S. and Lizaso, J. I.: Putting mechanisms into crop production models: Putting mechanisms into crop production models, Plant Cell Environ., 36(9), 1658–1672, doi:10.1111/pce.12119, 2013.

van Bussel, L. G. J., Stehfest, E., Siebert, S., Müller, C. and Ewert, F.: Simulation of the phenological development of wheat and maize at the global scale: Simulation of crop phenology at global scale, Glob. Ecol. Biogeogr., 24(9), 1018–1029, doi:10.1111/geb.12351, 2015a.

Deryng, D., Sacks, W. J., Barford, C. C. and Ramankutty, N.: Simulating the effects of climate and agricultural management practices on global crop yield: SIMULATING GLOBAL CROP YIELD, Glob. Biogeochem. Cycles, 25(2), n/a-n/a, doi:10.1029/2009GB003765, 2011.

Drewniak, B., Song, J., Prell, J., Kotamarthi, V. R. and Jacob, R.: Modeling agriculture in the Community Land Model, Geosci. Model Dev., 6(2), 495–515, doi:10.5194/gmd-6-495-2013, 2013.

Elliott, J., Kelly, D., Chryssanthacopoulos, J., Glotter, M., Jhunjhnuwala, K., Best, N., Wilde, M. and Foster, I.: The parallel system for integrating impact models and sectors (pSIMS), Environ.

https://doi.org/10.5194/gmd-2020-113
Preprint. Discussion started: 24 June 2020
© Author(s) 2020. CC BY 4.0 License.

Model. Softw., 62, 509–516, doi:https://doi.org/10.1016/j.envsoft.2014.04.008, 2014.

Elliott, J., Müller, C., Deryng, D., Chryssanthacopoulos, J., Boote, K. J., Büchner, M., Foster, I., Glotter, M., Heinke, J., Iizumi, T., Izaurralde, R. C., Mueller, N. D., Ray, D. K., Rosenzweig, C., Ruane, A. C. and Sheffield, J.: The Global Gridded Crop Model Intercomparison: data and modeling protocols for Phase 1 (v1.0), Geosci. Model Dev., 8(2), 261–277, doi:10.5194/gmd-8-261-2015, 2015.

Folberth, C., Gaiser, T., Abbaspour, K. C., Schulin, R. and Yang, H.: Regionalization of a large-scale crop growth model for sub-Saharan Africa: Model setup, evaluation, and estimation of maize yields, Agric. Ecosyst. Environ., 151, 21–33, doi:https://doi.org/10.1016/j.agee.2012.01.026, 2012.

Folberth, C., Skalský, R., Moltchanova, E., Balkovič, J., Azevedo, L. B., Obersteiner, M. and van der Velde, M.: Uncertainty in soil data can outweigh climate impact signals in global crop yield simulations, Nat. Commun., 7(1), doi:10.1038/ncomms11872, 2016.

Folberth, C., Elliott, J., Müller, C., Balkovič, J., Chryssanthacopoulos, J., Izaurralde, R. C., Jones, C. D., Khabarov, N., Liu, W., Reddy, A., Schmid, E., Skalský, R., Yang, H., Arneth, A., Ciais, P., Deryng, D., Lawrence, P. J., Olin, S., Pugh, T. A. M., Ruane, A. C. and Wang, X.: Parameterization-induced uncertainties and impacts of crop management harmonization in a global gridded crop model ensemble, edited by J. M. Martínez-Paz, PLOS ONE, 14(9), e0221862, doi:10.1371/journal.pone.0221862, 2019.

Gbegbelegbe, S., Cammarano, D., Asseng, S., Robertson, R., Chung, U., Adam, M., Abdalla, O., Payne, T., Reynolds, M., Sonder, K., Shiferaw, B. and Nelson, G.: Baseline simulation for global wheat production with CIMMYT mega-environment specific cultivars, Field Crops Res., 202, 122–135, doi:10.1016/j.fcr.2016.06.010, 2017.

Grassini, P., Thorburn, J., Burr, C. and Cassman, K. G.: High-yield irrigated maize in the Western U.S. Corn Belt: I. On-farm yield, yield potential, and impact of agronomic practices, Field Crops Res., 120(1), 142–150, doi:10.1016/j.fcr.2010.09.012, 2011.

van Ittersum, M. K., Cassman, K. G., Grassini, P., Wolf, J., Tittonell, P. and Hochman, Z.: Yield gap analysis with local to global relevance—A review, Field Crops Res., 143, 4–17, doi:10.1016/j.fcr.2012.09.009, 2013.

Izaurralde, R. C., Williams, J. R., McGill, W. B., Rosenberg, N. J. and Jakas, M. C. Q.: Simulating soil C dynamics with EPIC: Model description and testing against long-term data, Ecol. Model., 192(3), 362–384, doi:https://doi.org/10.1016/j.ecolmodel.2005.07.010, 2006.

Jones, J. W., Hoogenboom, G., Porter, C. H., Boote, K. J., Batchelor, W. D., Hunt, L. A., Wilkens, P. W., Singh, U., Gijsman, A. J. and Ritchie, J. T.: The DSSAT cropping system model, Eur. J. Agron., 18(3), 235–265, doi:https://doi.org/10.1016/S1161-0301(02)00107-7, 2003.

Keating, B. A., Carberry, P. S., Hammer, G. L., Probert, M. E., Robertson, M. J., Holzworth, D., Huth, N. I., Hargreaves, J. N., Meinke, H. and Hochman, Z.: An overview of APSIM, a model designed for farming systems simulation, Eur. J. Agron., 18(3–4), 267–288, 2003.

Kiniry, J. R., Jones, C. A., O'toole, J. C., Blanchet, R., Cabelguenne, M. and Spanel, D. A.: Radiation-use efficiency in biomass accumulation prior to grain-filling for five grain-crop species, Field Crops Res., 20(1), 51–64, 1989.

https://doi.org/10.5194/gmd-2020-113
Preprint. Discussion started: 24 June 2020
© Author(s) 2020. CC BY 4.0 License.

Lindeskog, M., Arneth, A., Bondeau, A., Waha, K., Seaquist, J., Olin, S. and Smith, B.: Implications of accounting for land use in simulations of ecosystem carbon cycling in Africa, Earth Syst. Dyn., 4(2), 385–407, doi:10.5194/esd-4-385-2013, 2013.

Liu, J., Williams, J. R., Zehnder, A. J. B. and Yang, H.: GEPIC – modelling wheat yield and crop water productivity with high resolution on a global scale, Agric. Syst., 94(2), 478–493, doi:10.1016/j.agsy.2006.11.019, 2007.

Lobell, D. B., Cassman, K. G. and Field, C. B.: Crop yield gaps: their importance, magnitudes, and causes, Annu. Rev. Environ. Resour., 34(1), 179, 2009.

Martre, P., Wallach, D., Asseng, S., Ewert, F., Jones, J. W., Rötter, R. P., Boote, K. J., Ruane, A. C., Thorburn, P. J., Cammarano, D., Hatfield, J. L., Rosenzweig, C., Aggarwal, P. K., Angulo, C., Basso, B., Bertuzzi, P., Biernath, C., Brisson, N., Challinor, A. J., Doltra, J., Gayler, S., Goldberg, R., Grant, R. F., Heng, L., Hooker, J., Hunt, L. A., Ingwersen, J., Izaurralde, R. C., Kersebaum, K. C., Müller, C., Kumar, S. N., Nendel, C., O'leary, G., Olesen, J. E., Osborne, T. M., Palosuo, T., Priesack, E., Ripoche, D., Semenov, M. A., Shcherbak, I., Steduto, P., Stöckle, C. O., Stratonovitch, P., Streck, T., Supit, I., Tao, F., Travasso, M., Waha, K., White, J. W. and Wolf, J.: Multimodel ensembles of wheat growth: many models are better than one, Glob. Change Biol., 21(2), 911–925, doi:10.1111/gcb.12768, 2015.

Minoli, S., Müller, C., Elliott, J., Ruane, A. C., Jägermeyr, J., Zabel, F., Dury, M., Folberth, C., François, L., Hank, T., Jacquemin, I., Liu, W., Olin, S. and Pugh, T. A. M.: Global Response Patterns of Major Rainfed Crops to Adaptation by Maintaining Current Growing Periods and Irrigation, Earths Future, 7(12), 1464–1480, doi:10.1029/2018EF001130, 2019.

Mueller, N. D., Gerber, J. S., Johnston, M., Ray, D. K., Ramankutty, N. and Foley, J. A.: Closing yield gaps through nutrient and water management, Nature, 490(7419), 254–257, doi:10.1038/nature11420, 2012.

Müller, C., Elliott, J., Kelly, D., Arneth, A., Balkovic, J., Ciais, P., Deryng, D., Folberth, C., Hoek, S., Izaurralde, R. C., Jones, C. D., Khabarov, N., Lawrence, P., Liu, W., Olin, S., Pugh, T. A. M., Reddy, A., Rosenzweig, C., Ruane, A. C., Sakurai, G., Schmid, E., Skalsky, R., Wang, X., de Wit, A. and Yang, H.: The Global Gridded Crop Model Intercomparison phase 1 simulation dataset, Sci. Data, 6(1), doi:10.1038/s41597-019-0023-8, 2019a.

Müller, C., Elliott, J., Kelly, D., Arneth, A., Balkovic, J., Ciais, P., Deryng, D., Folberth, C., Hoek, S., Izaurralde, R. C., Jones, C. D., Khabarov, N., Lawrence, P., Liu, W., Olin, S., Pugh, T. A. M., Reddy, A., Rosenzweig, C., Ruane, A. C., Sakurai, G., Schmid, E., Skalsky, R., Wang, X., de Wit, A. and Yang, H.: The Global Gridded Crop Model Intercomparison phase 1 simulation dataset, Sci. Data, 6(1), doi:10.1038/s41597-019-0023-8, 2019b.

Padilla, J. M. and Otegui, M. E.: Co-ordination between Leaf Initiation and Leaf Appearance in Field-grown Maize (Zea mays): Genotypic Differences in Response of Rates to Temperature, Ann. Bot., 96(6), 997–1007, doi:10.1093/aob/mci251, 2005.

Portmann, F. T., Siebert, S. and Döll, P.: MIRCA2000-Global monthly irrigated and rainfed crop areas around the year 2000: A new high-resolution data set for agricultural and hydrological modeling: MONTHLY IRRIGATED AND RAINFED CROP AREAS, Glob. Biogeochem. Cycles, 24(1), n/a-n/a, doi:10.1029/2008GB003435, 2010.

Ruane, A. C., Goldberg, R. and Chryssanthacopoulos, J.: Climate forcing datasets for agricultural

https://doi.org/10.5194/gmd-2020-113
Preprint. Discussion started: 24 June 2020
© Author(s) 2020. CC BY 4.0 License.

modeling: Merged products for gap-filling and historical climate series estimation, Agric. For. Meteorol., 200, 233–248, doi:https://doi.org/10.1016/j.agrformet.2014.09.016, 2015.

Sacks, W. J., Deryng, D., Foley, J. A. and Ramankutty, N.: Crop planting dates: an analysis of global patterns, Glob. Ecol. Biogeogr., 19(5), 607–620, doi:10.1111/j.1466-8238.2010.00551.x, 2010.

Sangoi, L., Gracietti, M. A., Rampazzo, C. and Bianchetti, P.: Response of Brazilian maize hybrids from different eras to changes in plant density, Field Crops Res., 79(1), 39–51, 2002.

Schaphoff, S., von Bloh, W., Rammig, A., Thonicke, K., Biemans, H., Forkel, M., Gerten, D., Heinke, J., Jägermeyr, J., Knauer, J., Langerwisch, F., Lucht, W., Müller, C., Rolinski, S. and Waha, K.: LPJmL4 – a dynamic global vegetation model with managed land – Part 1: Model description, Geosci. Model Dev., 11(4), 1343–1375, doi:10.5194/gmd-11-1343-2018, 2018a.

Schaphoff, S., Forkel, M., Müller, C., Knauer, J., von Bloh, W., Gerten, D., Jägermeyr, J., Lucht, W., Rammig, A., Thonicke, K. and Waha, K.: LPJmL4 – a dynamic global vegetation model with managed land – Part 2: Model evaluation, Geosci. Model Dev., 11(4), 1377–1403, doi:10.5194/gmd-11-1377-2018, 2018b.

Sinclair, T. R. and Muchow, R. C.: Radiation Use Efficiency, Adv. Agron., 215–265, 1999.

Smith, B., Prentice, I. C. and Sykes, M. T.: Representation of vegetation dynamics in the modelling of terrestrial ecosystems: comparing two contrasting approaches within European climate space, Glob. Ecol. Biogeogr., 10(6), 621–637, doi:10.1046/j.1466-822X.2001.t01-1-00256.x, 2001.

Testa, G., Reyneri, A. and Blandino, M.: Maize grain yield enhancement through high plant density cultivation with different inter-row and intra-row spacings, Eur. J. Agron., 72, 28–37, doi:10.1016/j.eja.2015.09.006, 2016.

van Bussel, L. G. J., Grassini, P., Van Wart, J., Wolf, J., Claessens, L., Yang, H., Boogaard, H., de Groot, H., Saito, K., Cassman, K. G. and van Ittersum, M. K.: From field to atlas: Upscaling of location-specific yield gap estimates, Field Crops Res., 177, 98–108, doi:10.1016/j.fcr.2015.03.005, 2015b.

Waha, K., van Bussel, L. G. J., Müller, C. and Bondeau, A.: Climate-driven simulation of global crop sowing dates: Simulation of global sowing dates, Glob. Ecol. Biogeogr., 21(2), 247–259, doi:10.1111/j.1466-8238.2011.00678.x, 2012.

Wang, E., Robertson, M. J., Hammer, G. L., Carberry, P. S., Holzworth, D., Meinke, H., Chapman, S. C., Hargreaves, J. N. G., Huth, N. I. and McLean, G.: Development of a generic crop model template in the cropping system model APSIM, Eur. J. Agron., 18(1–2), 121–140, doi:10.1016/S1161-0301(02)00100-4, 2002.

Williams, J. R. In Computer models of watershed hydrology (Singh, V. P. ed.) 909–1000 (Water Resources Publications, 1995)

https://doi.org/10.5194/gmd-2020-113
Preprint. Discussion started: 24 June 2020
© Author(s) 2020. CC BY 4.0 License.

Geoscientific Model Development
Discussions
Open Access
EGU

Main Figures

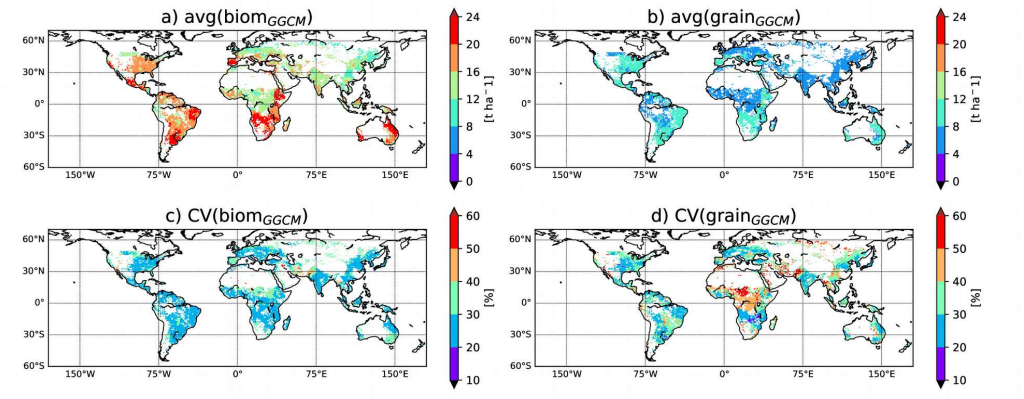

Fig.1: GGCM divergence in simulation of potential aboveground biomass and yield. Average and coefficient of variation for both aboveground biomass (*biom*) and yield (*grain*) computed among 8 GGCMs used in the current analysis for simulations approaching potential yield in GGCMI (i.e. *harmnon* x *irrigated* for LPJ-GUESS, LPJmL, CLM-crop, pDSSAT, pAPSIM, GEPIC, EPIC-IIASA and *default* x *irrigated* for CGMS-WOFOST; see Sect.2.2.1). Only grid-cells common to the 8 GGCMs are considered for the figure. For GEPIC and EPIC-IIASA, the variable *biom* has been corrected (see Sect.2.2.1). For the comparison including in addition GGCMs that provide *biom* and *grain* for *harmnon* x *irrigated* simulation in GGCMI but which are not part of the current manuscript (i.e. EPIC-BOKU, PEPIC, PEGASUS), see Fig.S1.

https://doi.org/10.5194/gmd-2020-113
Preprint. Discussion started: 24 June 2020
© Author(s) 2020. CC BY 4.0 License.

Geoscientific Model Development
Discussions
Open Access
EGU

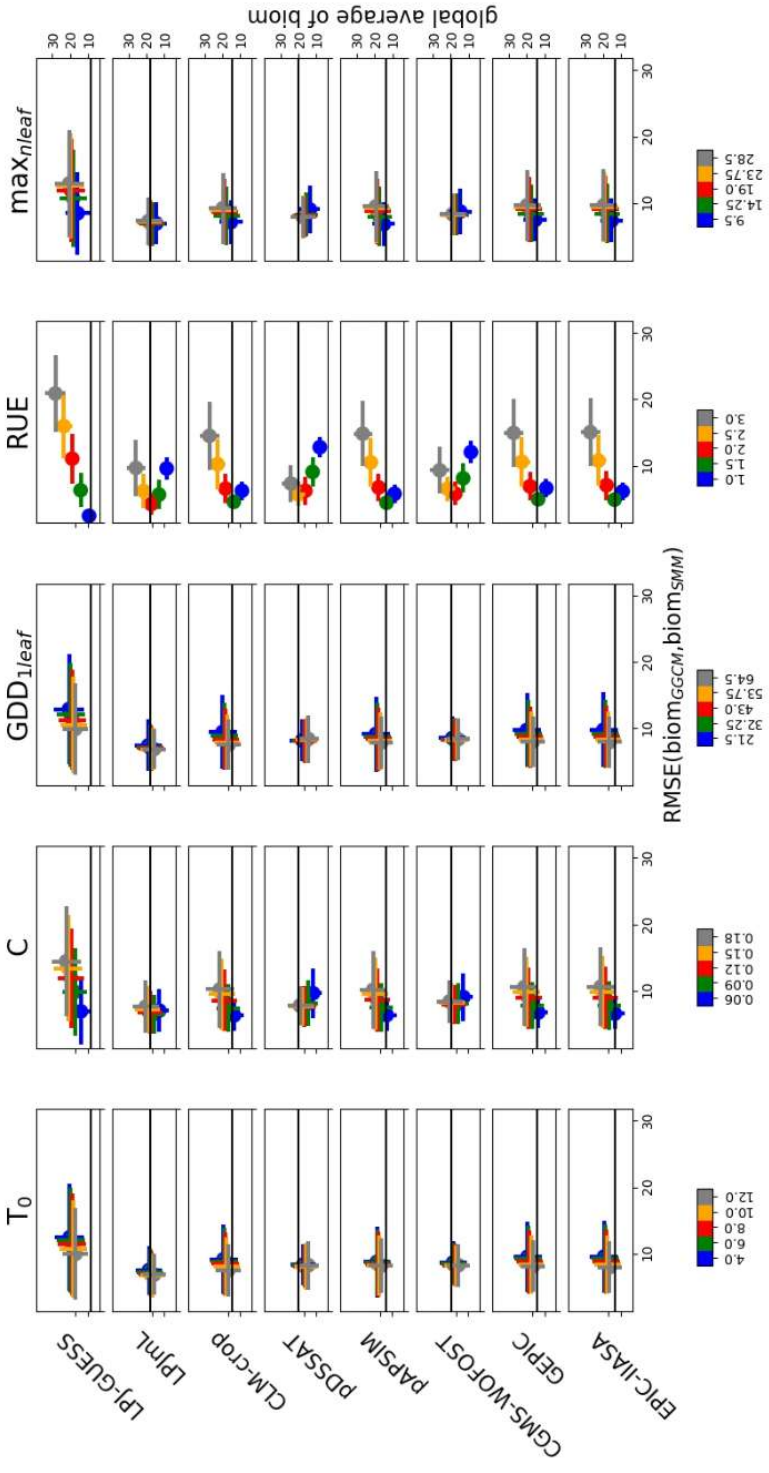

https://doi.org/10.5194/gmd-2020-113
Preprint. Discussion started: 24 June 2020
© Author(s) 2020. CC BY 4.0 License.

Geoscientific Model Development Discussions
Open Access
EGU

Fig.2: Global RMSE ($biom_{SMM}$,$biom_{GGCM}$) and global averaged $biom_{SMM}$: sensitivity to SMM parameters. Five different values are used for each SMM parameter and thus, 5^5 SMM simulations have been performed. The different lines correspond to the different GGCMs. For a given line, and for a given column (i.e. for a given SMM parameter), each dot represents all SMM simulations sharing the same value for this parameter, which defines its color. Error-bars corresponds to the standard deviation among these SMM simulations. Each dot is defined through the RMSE($biom_{GGCM}$,$biom_{SMM}$) (x-axis, in [t ha^{-1}]) and the global averaged $biom_{SMM}$ (y-axis, in [t ha^{-1}]). The black horizontal line reports the global averaged $biom_{GGCM}$ on y-axis. The difference of $biom_{SMM}$ between rows for a given column results from differences in growth periods between GGCMs (and in a lesser extent from difference in the spatial coverage of maize between GGCMs). Global values (average, RMSE) are computed by giving the same weight to each grid-cell.

https://doi.org/10.5194/gmd-2020-113
Preprint. Discussion started: 24 June 2020
© Author(s) 2020. CC BY 4.0 License.

Geoscientific Model Development
Discussions
Open Access
EGU

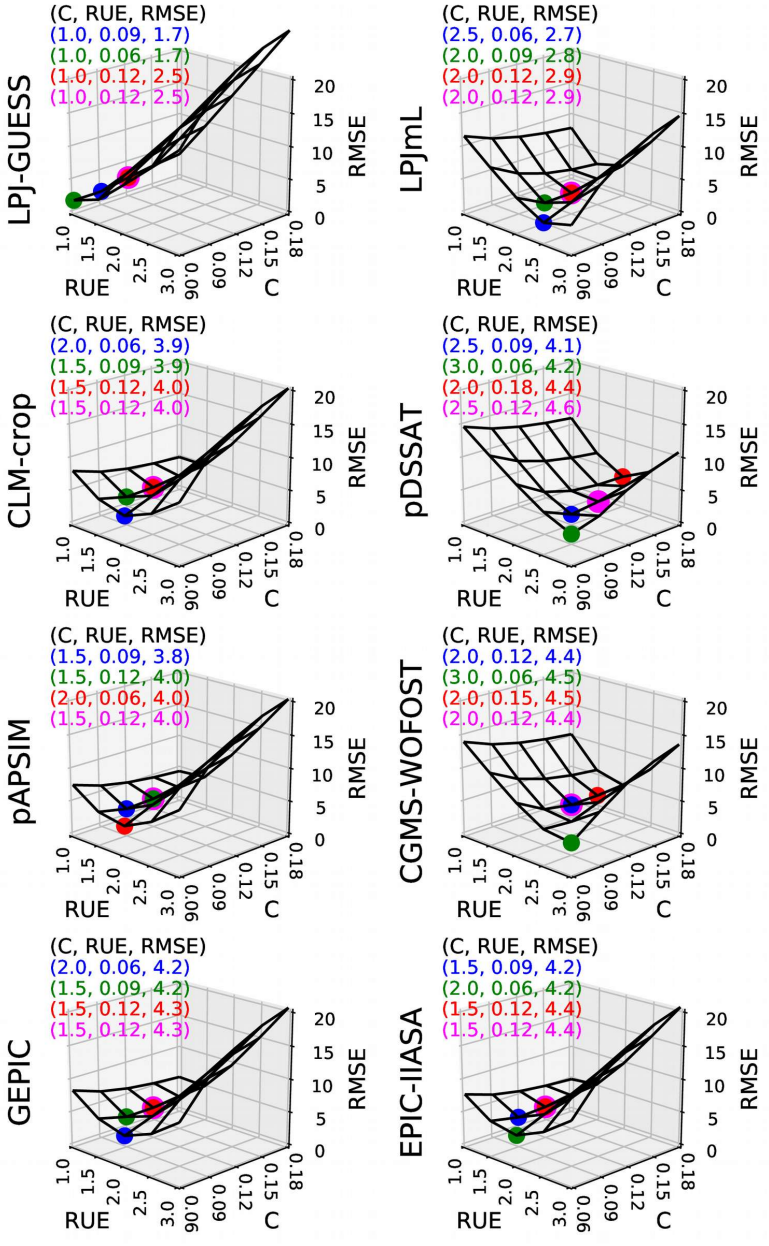

Fig.3: Sensitivity of global RMSE ($biom_{SMM}$,$biom_{GGCM}$) (t DM ha^{-1}) to *C* (-) and *RUE* (g DM MJ^{-1}) for each GGCM. For each GGCM, the shape of RMSE is derived from 25 SMM simulations (5 values of *C* combined with 5 values of *RUE*). Other SMM parameters are equal to their respective initial estimate. For each GGCM, 3 (*C, RUE*) pairs that minimize the most RMSE among the 25 pairs tested are plotted in blue, green, red. A fourth (*C*, *RUE*) pair minimizing the RMSE but with *C* equal to its initial estimate is in magenta. The values of the four (*C, RUE*) pairs and the corresponding RMSE are given in top left of each panel.

https://doi.org/10.5194/gmd-2020-113
Preprint. Discussion started: 24 June 2020
© Author(s) 2020. CC BY 4.0 License.

Geoscientific Model Development
Discussions
Open Access
EGU

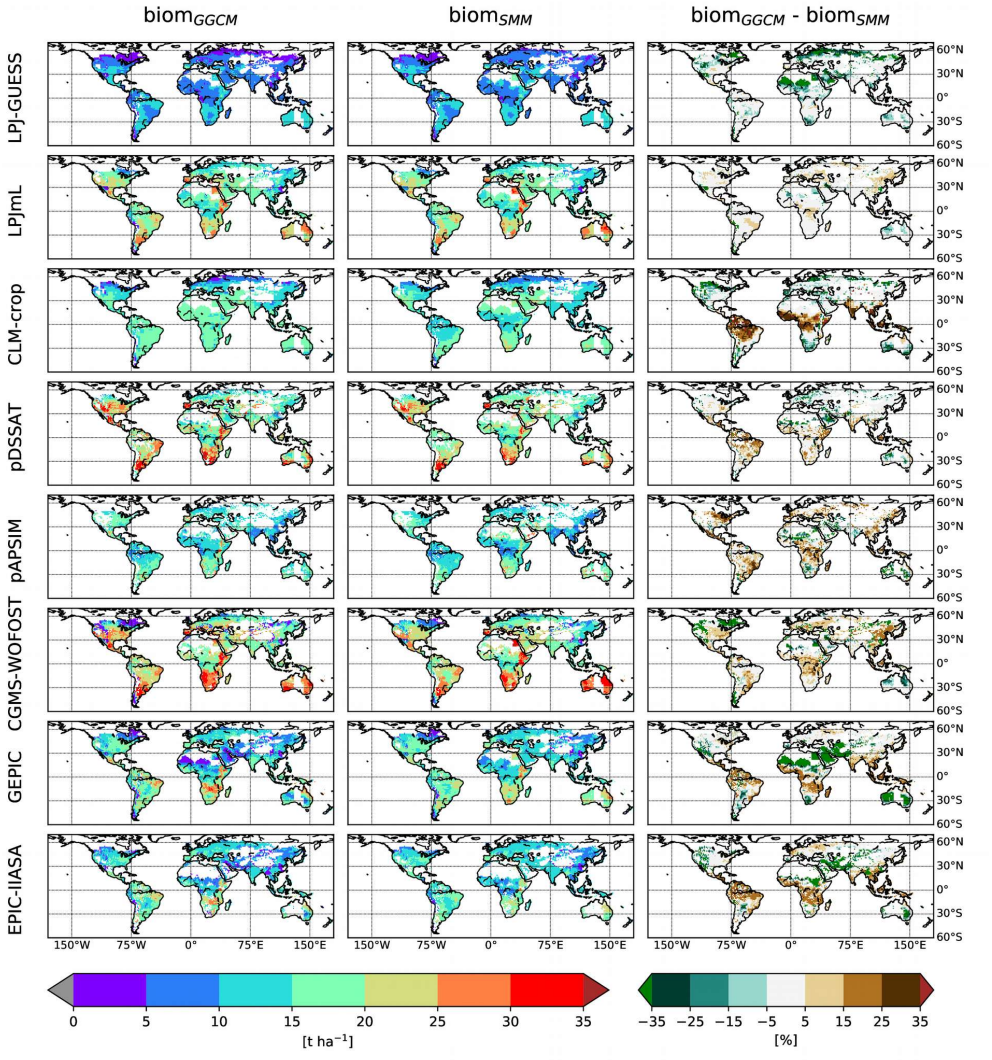

Fig.4: Comparison of the spatial distribution of simulated aboveground biomass (*biom*) between GGCM and SMM after its calibration. For each GGCM (row), the figure displays $biom_{GGCM}$ (left column), $biom_{SMM}$ after SMM calibration (i.e. calibration of global GGCM-dependent *C* and *RUE* and spatial varying GDD_{1leaf}) and the difference ($biom_{GGCM}$ - $biom_{SMM}$) (expressed in percent of $biom_{GGCM}$). Only $biom_{SMM}$ after SMM calibration for the 1st (*C, RUE*) pair is shown.

https://doi.org/10.5194/gmd-2020-113
Preprint. Discussion started: 24 June 2020
© Author(s) 2020. CC BY 4.0 License.

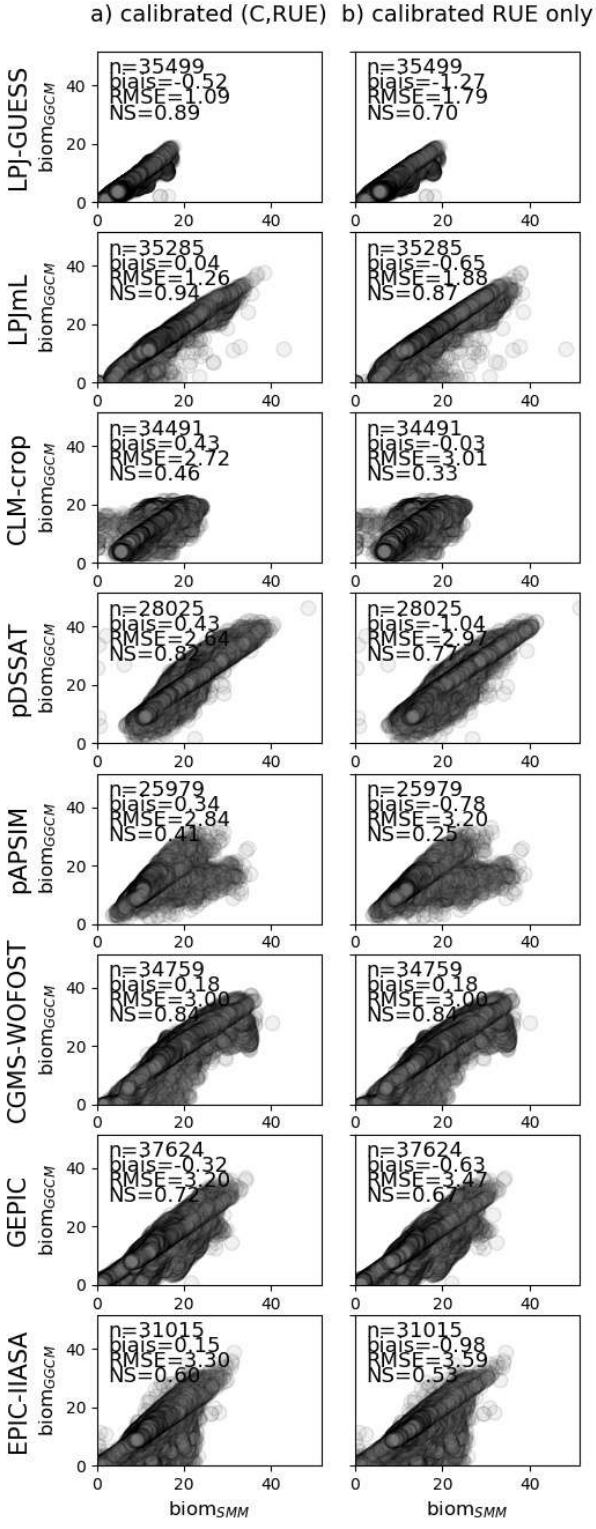

Fig.5: Scatter-plots of $biom_{GGCM}$ (y-axis) vs $biom_{SMM}$ (x-axis) after SMM calibration, i.e. calibration of global GGCM-dependent (*C*, *RUE*) and spatial varying GDD_{1leaf}. In left column (a), the (*C*, *RUE*) pair that minimizes the most the RMSE is used while in right column (b), the (*C*, *RUE*) minimizing the RMSE with *C* equal to its initial estimate (so called 4th pair in Sect. 2.2.4.1) is used. Each dot corresponds to one grid-cell. In top left of each panel, the number of grid-cells considered (n), as well as different quantifications of the SMM vs GGCM agreement (bias, RMSE and Nash-Sutcliffe coefficient - NS) are given. See Fig.S6 for scatter-plots with the four (*C*, *RUE*) pairs.

https://doi.org/10.5194/gmd-2020-113
Preprint. Discussion started: 24 June 2020
© Author(s) 2020. CC BY 4.0 License.

Geoscientific Model Development Discussions
Open Access
EGU

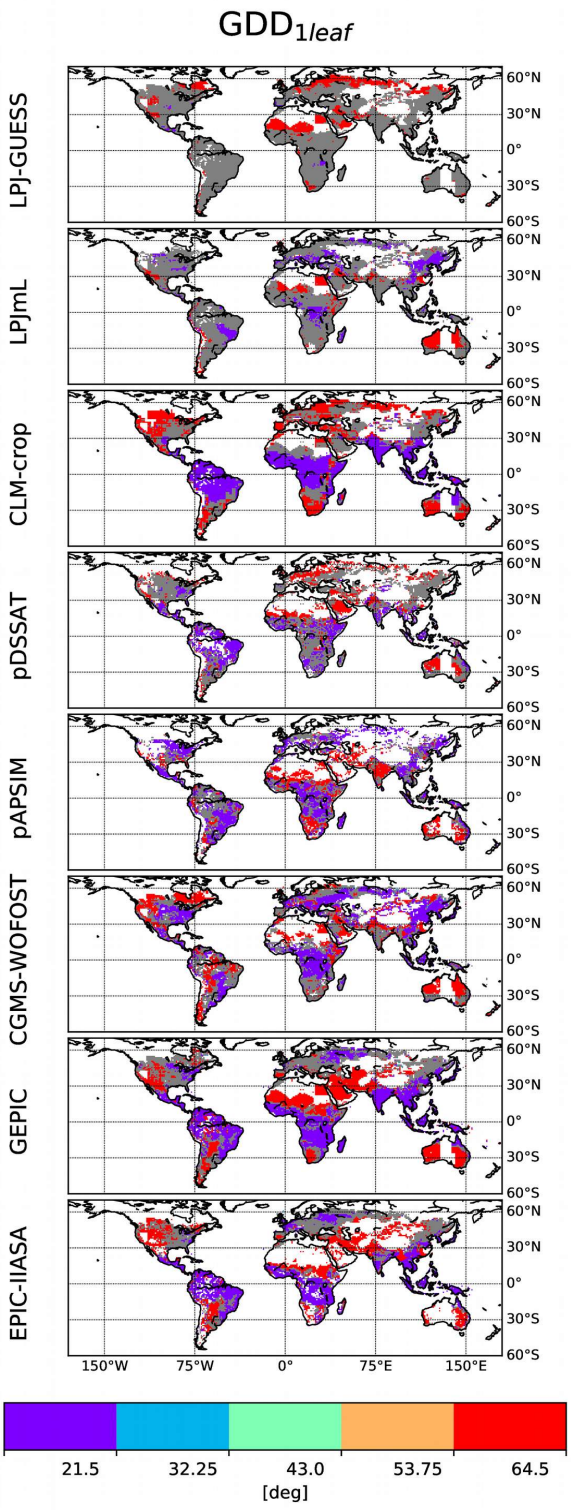

Fig.6: Calibrated spatial distribution of GDD_{1leaf}. Five values of GDD_{1leaf} are allowed (color-palet and Table S1). Global GGCM-dependent (*C*, *RUE*) have been calibrated prior to GDD_{1leaf} and for a given GGCM, grid-cells for which calibrated GDD_{1leaf} are different for the four (*C*, *RUE*) pairs are in grey.

https://doi.org/10.5194/gmd-2020-113
Preprint. Discussion started: 24 June 2020
© Author(s) 2020. CC BY 4.0 License.

Geoscientific Model Development Discussions

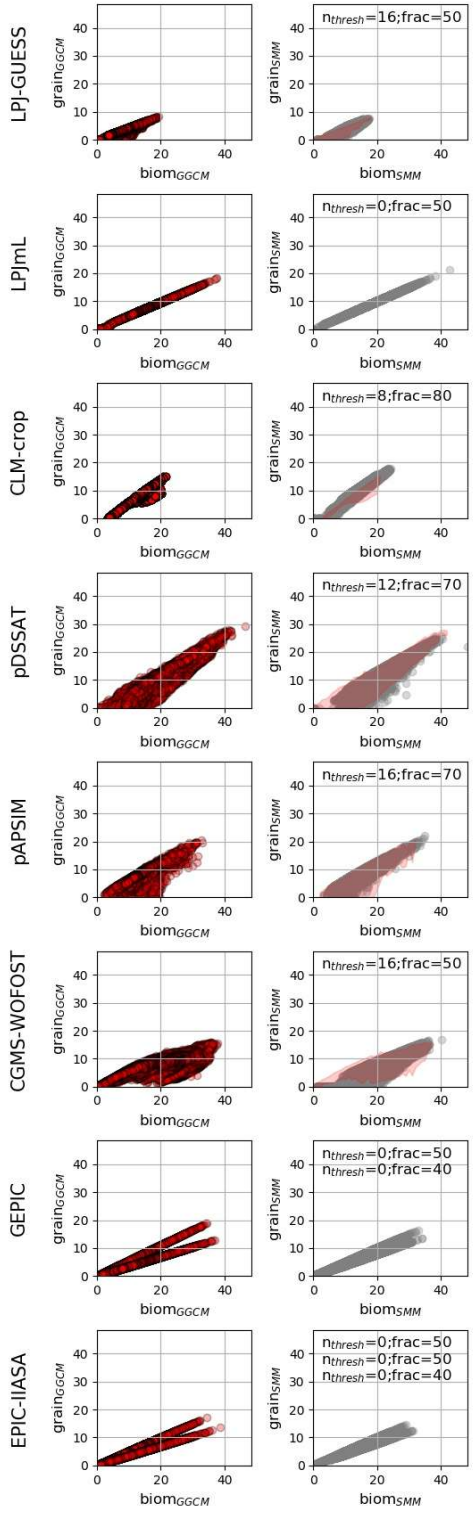

Fig.7: Relationship between *grain* and *biom*: comparison between GGCM and SMM after its calibration. The figure displays the *grain* vs. *biom* relationship for GGCMs (left column) and for SMM after independent calibration against each GGCM (right column). For SMM, the relationship is given for the (n_{thresh}, *frac*) combination that maximizes the match between GGCM and SMM (see Methods). Calibrated combination is given in top of each SMM panel. When multiple cultivars are considered, one calibrated (n_{thresh}, *frac*) combination is given per cultivar. In right panels, pink shading defines A_{GGCM} (see Methods).

https://doi.org/10.5194/gmd-2020-113
Preprint. Discussion started: 24 June 2020
© Author(s) 2020. CC BY 4.0 License.

Geoscientific Model Development
Discussions
Open Access
EGU

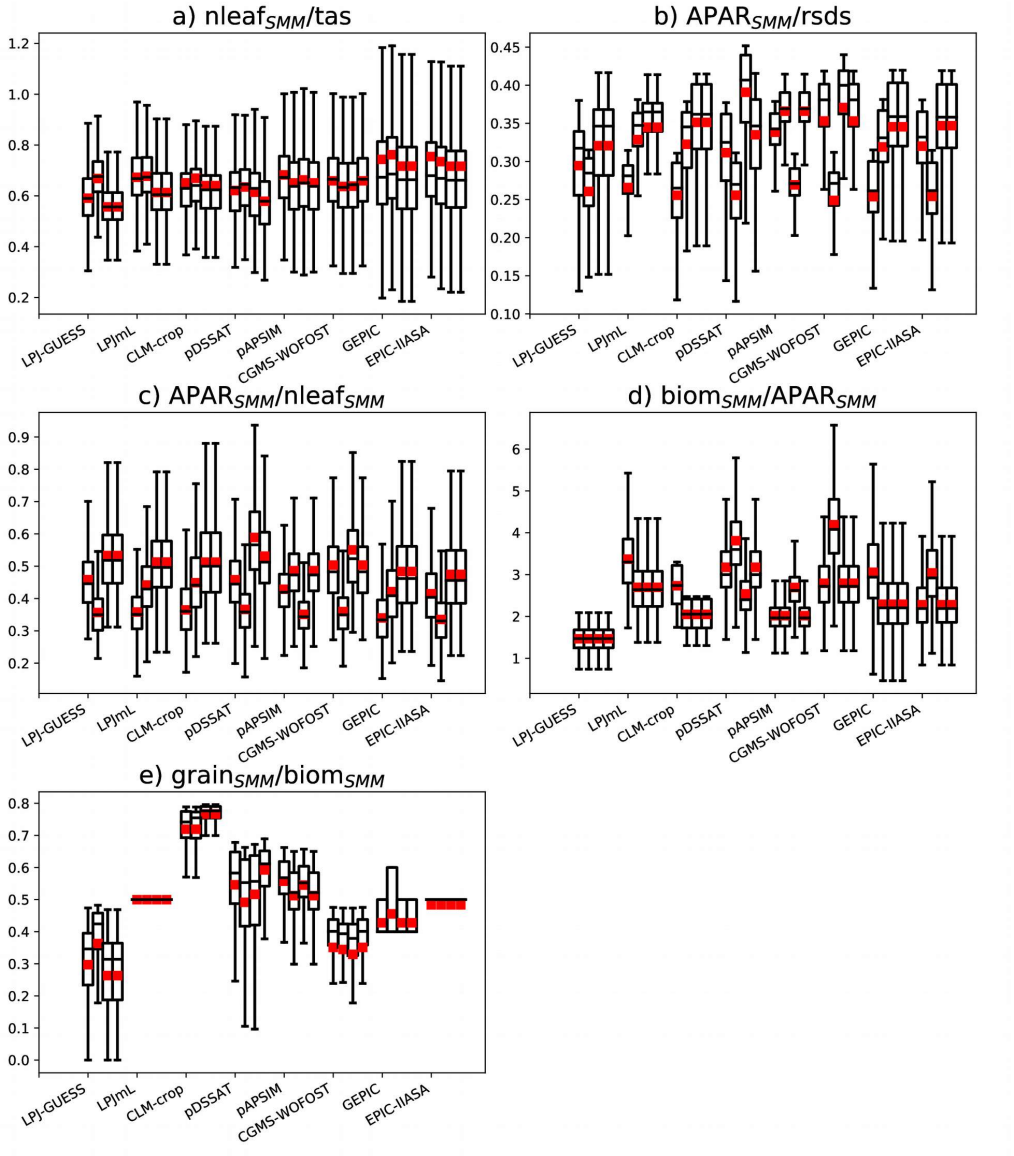

Fig.8: Barplots of different ratios computed with SMM calibrated against each GGCM. Each panel shows a ratio (a: n_{leaf}/tas, b: $APAR/rsds$, c: $APAR/n_{leaf}$, d: $biom/APAR$, e: $grain/biom$) while for a given panel, x-ticks correspond to emulated GGCMs. Four different (*C, RUE*) pairs have been tested and correspond to the 4 bars of each x-tick.